A theoretical simulation model for optimization of fins on the shell of a hermetic reciprocating compressor

IOP Conf. Series: Materials Science and Engineering **604** (2019) 012028 doi:10.1088/1757-899X/604/1/012028

A theoretical simulation model for optimization of fins on the shell of a hermetic reciprocating compressor

T Dutra[1], **S Moratelli**
Department of Energy and Sustainability, Federal University of Santa Catarina, Ararangua, SC, Brazil

E-mail: dutra.thiago@ufsc.br

Abstract. The cost of a hermetic reciprocating compressor is quite dependent on the electric motor employed to drive it. Usually, the higher the motor efficiency, the higher the costs. Therefore, some compressors are designed to operate with low-efficiency electric motors. The main difficulty in such a case is to ensure that the motor operates at a temperature below the upper threshold. This paper presents a simulation model for optimization of fins on the shell of a hermetic reciprocating compressor which operates with a low-efficiency motor. The objective of the simulation is to obtain a set of fins with minimum volume that allows the compressor to operate under a critical operating condition without overheating the electric motor. The simulation model is implemented by coupling a lumped-parameter thermal simulation model of the reciprocating compressor with an optimization algorithm. The results of the thermal simulation are validated with experimental data. Different fin profiles are considered in the analysis. It is concluded that the optimum heat sink solution is conditioned to the minimum fin thickness or to the minimum fin diameter allowed, which are dependent on other compressor design constraints.

1. Introduction

The design of hermetic reciprocating compressors is driven by cost, efficiency, reliability and noise issues. In general, the higher the compressor efficiency the higher the costs, which are quite dependent on the electric motor costs. In some cases, it is convenient to design less efficient compressors driven by low-efficiency electric motors. These compressors require a high power input for shaft power generation, bringing about a large heat dissipation rate and rising the temperature of internal parts (such as suction gas, electric motor and bearings). The increase of the suction gas temperature results in a decrease of compressor volumetric and isentropic efficiencies. Moreover, reliability issues may arise from electric motor overheating, such as the deterioration of the winding insulation. Therefore, thermal management solutions are necessary to ensure the motor temperature does not surpass the upper threshold. Such solutions can be assessed from thermal simulation models.

Lumped-parameter thermal models have been developed to predict the temperature distribution in components of hermetic compressors. In these models, control volumes are assigned to compressor components and the energy conservation equation is applied to each one. Thermal conductances are established between the control volumes and are obtained from experimental data [1, 2] or heat transfer correlations for simplified geometries [3, 4]. Ooi [5] developed a lumped-parameter thermal-model for a reciprocating compressor and used it to assess thermal management solutions, such as the modification of materials and repositioning of the suction muffler to decrease the suction gas temperature and improve

[1] To whom any correspondence should be addressed.

the compressor efficiency. He et al. [6], Dutra and Deschamps [7, 8] proposed simulation models for a semi-hermetic screw compressor and a hermetic reciprocating compressor, respectively, and employed them to evaluate the influence of operating conditions and geometric parameters on the electric motor temperature. Specifically in the work of Dutra and Deschamps [8], the simulation model was used to investigate the increase of electric motor temperature as motor efficiency is decreased by reducing the stator winding wire diameter.

Distributed-parameter thermal models allow a more detailed characterization of the heat transfer. Kara and Oguz [9] used a commercial package based on the finite volume method (FVM) to solve the heat conduction equation in the solid parts of a reciprocating compressor. Birari et al. [10] built a FVM model to solve the fluid flow and the heat transfer in a reciprocating compressor. Oliveira et al. [11] carried out a similar work in an oil-free linear compressor and used the model to investigate the sensitivity of the suction gas temperature with respect to different materials adopted in the insulating gasket. Schreiner et al. [12] and Posch et al. [13] employed hybrid lumped-distributed-parameter thermal-models to assess the effect of virtual heat sinks positioned in the crankcase to reduce the suction gas temperature in hermetic reciprocating compressors. Other papers [14-16] adopted FVM models to predict the temperature distribution in electric motors of hermetic compressors. Such works highlight the importance of maintaining the motor temperature below a specific value, but apply the simulation models solely to investigate the effect of heat transfer mechanisms and to predict the temperature gradient in the electric motor, rather than evaluating thermal management solutions.

Although many papers in the literature concern the thermal simulation of compressors, a few of them focus on assessing thermal management solutions. From these works, most are concerned with the reduction of suction gas superheating to improve volumetric and isentropic efficiencies [5, 11, 12, 13]. According to [13], the most common strategy adopted to reduce the temperature of the electric motor in a hermetic compressor is to make the refrigerant gas to flow over the motor before being suctioned by the compression chamber. However, such a solution results in decrease of volumetric and isentropic efficiencies, as the temperature of the suction gas increases when cooling the motor. Other common solution is to use a fan to cool down the compressor, but at the expense of an additional power consumption. An additional alternative for the thermal management of the electric motor is the attachment of fins to the external side of the compressor shell. Schreiner [17] carried out an optimization of annular fins in the shell of a reciprocating compressor adopted for refrigeration. A hybrid lumped-distributed parameter thermal-model was used to implement the thermal management solution, and a reduction of 13°C in the mean temperature of the motor was observed when the optimum configuration of fins is adopted at natural convection condition.

Finned shells are not commonly adopted in refrigeration hermetic compressors. On the other hand, there is a lack of information in the literature concerning the potential of such a thermal management solution for this specific application. Thus, this paper presents a simplified simulation model for optimization of fins on the shell of a hermetic reciprocating compressor. The objective of this model is to obtain a set of fins with minimum volume (or amount of material) that ensures motor operating temperature below an upper threshold. The simulation model is formed by the integration of a compressor lumped thermal-model with an optimization algorithm. The thermal model is validated with data available in the literature. Pin- and rectangular-fin profiles are evaluated and the results are discussed. It should be mentioned that this paper is not intended to discuss the feasibility of implementing the solution, which is dependent on manufacture process constraints.

2. Simulation model

First, a compressor thermal model based on the paper of Dutra and Deschamps [7] is implemented. Some changes are made in order to include the effect of the fins attached to the compressor shell. Finally, the optimization algorithm is coupled to the thermal model and the simulation is carried out.

2.1. Thermal model

The thermal model follows the steady-state lumped formulation of the energy conservation equation [7]:

$$\dot{Q}_i - \dot{W}_i = \sum (\dot{m}h)_{i,in} - \sum (\dot{m}h)_{i,out} \quad (1)$$

where $\dot{Q}_i$ represents the heat transfer rate between the element i and its surroundings, the rate of work associated with the element i is $\dot{W}_i$, and $\Sigma(\dot{m}h)_{i,in}$ and $\Sigma(\dot{m}h)_{i,out}$ denote the energy rate transported by the mass flow rate into and from the element i, respectively.

The hermetic compressor was divided into eight lumped elements: suction muffler (1), compression chamber (2), discharge chamber (3), discharge muffler (4), discharge tube (5), electric motor (6), internal environment (7) and shell (8). The internal environment refers to the fluid portion inside the compressor housing. Figure 1 shows a schematic of the lumped elements and the energy interactions between them.

Table 1 presents the terms of equation (1) associated with each one of the compressor elements. In the energy balance applied to the compression chamber (ID = 2), leakage and heat transfer through the cylinder wall are disregarded and $\dot{W}_{sh}$ ($=\eta_{ele}\ \dot{W}_{ele}$) denotes the shaft power. Input data for the energy balances are the mass flow rate ($\dot{m}$), the input power ($\dot{W}_{ele}$), the electric motor efficiency (η_{ele}) and the thermal conductances ($UA_{i,j}$), where i and j refer to lumped element indexes (ID). Mass flow rate and input power are obtained previously, using the volumetric and isentropic efficiencies, η_v and η_s:

$$\dot{m} = \eta_v \rho_{sl} V_{sw} f; \qquad \dot{W}_{ele} = \frac{\dot{m}(h^s - h_{sl})}{\eta_s} \quad (2)$$

where ρ_{sl} and h_{sl} are the gas density and specific enthalpy evaluated at the evaporating pressure and suction line temperature, respectively, and h^s is the specific enthalpy evaluated at the condensing pressure and suction line specific entropy. The compressor volumetric displacement is denoted by V_{sw} and f is the line frequency. Experimental data for electric motor efficiency, as well as for volumetric and isentropic efficiencies, were obtained from Dutra and Deschamps [7] for different operating conditions. The thermal conductances UA were computed from experimental data for a single operating condition.

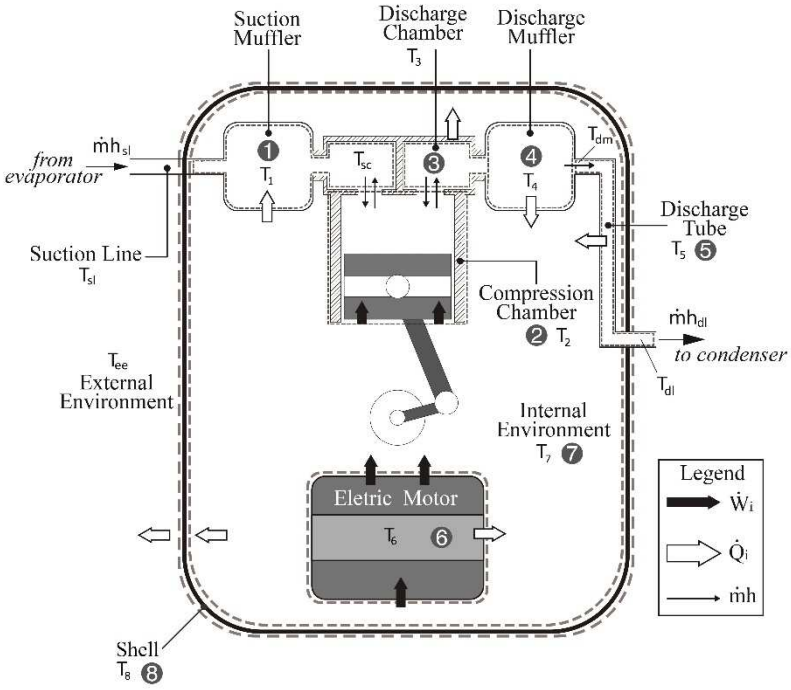

Figure 1. Schematic of the compressor lumped elements (adapted from Dutra and Deschamps [7]).

Table 1. Energy balance terms applied to the lumped elements.

ID	$\dot{Q}_i$	$\dot{W}_i$	$\sum(\dot{m}h)_{i,in}$	$\sum(\dot{m}h)_{i,out}$
1	$UA_{1,7}(T_1 - T_7)$	-	$\dot{m}h_{sl}$	$\dot{m}h_{sc}$
2	-	$\dot{W}_{sh}$	$\dot{m}h_{sc}$	$\dot{m}h_2$
3	$UA_{3,7}(T_3 - T_7)$	-	$\dot{m}h_2$	$\dot{m}h_3$
4	$UA_{4,7}(T_4 - T_7)$	-	$\dot{m}h_3$	$\dot{m}h_{dm}$
5	$UA_{5,7}(T_5 - T_7)$	-	$\dot{m}h_{dm}$	$\dot{m}h_{dl}$
6	$UA_{6,7}(T_6 - T_7)$	$\dot{W}_{ele}(1 - \eta_{ele})$	-	-
7	$\sum_1^8 UA_{i,7}(T_7 - T_i)$; for i≠ 2 *e* $i \neq 7$	-	-	-
8	$UA_{8,ee}(T_8 - T_{ee}) + UA_{8,7}(T_8 - T_7)$	-	-	-

The system of non-linear equations is solved via the Newton-Raphson method. The mean temperatures in the suction muffler, discharge muffler and discharge tube, denoted respectively by T_1, T_4 and T_5, are given by:

$$T_1=0.5(T_{sl}+T_{sc}); \qquad T_4=0.5(T_3+T_{dm}); \qquad T_5=0.5(T_{dm}+T_{dl}) \tag{3}$$

2.2. Optimization problem

The thermal conductance between the shell and the external environment ($UA_{8,ee}$) is initially adjusted with experimental data for a baseline compressor. To incorporate the fins to the thermal model, the energy balance applied to the shell must be slightly modified by replacing $UA_{8,ee}$ by $UA_{8,ee,f}$:

$$UA_{8,ee,f}=U\left(A_s - NA_{cs} + \eta_f NA_f\right) \tag{4}$$

where A_s denotes the compressor shell area before the installation of fins, A_{cs} is the fin cross-sectional area, A_f is the fin surface area, η_f is the fin efficiency, N represents the number of fins and U is the global heat transfer coefficient ($=UA_{8,ee}/A_s$), which is assumed constant. For the compressor considered herein, the shell area (A_s) was roughly estimated to be 0.1 m². Fin efficiency is computed as [18]:

$$\eta_f=\frac{\tanh\left(L_c\sqrt{UP/kA_{cs}}\right)}{L_c\sqrt{UP/kA_{cs}}} \tag{5}$$

where P is the fin perimeter, k is the fin thermal conductivity and L_c is the corrected fin length [19].

The heat transfer rate rejected by the compressor shell ($\dot{Q}_8$) can be written as:

$$\dot{Q}_8 = UA_{8,ee,f}(T_8 - T_{ee}) \tag{6}$$

Combining equation (6) with equation (4) and additional relations available in Table 1 for T_8 ($= T_7 - \dot{Q}_8/UA_{8,7}$) and for T_7 ($= T_6 - \dot{Q}_6/UA_{6,7}$), one obtains:

$$N = \frac{1}{A_{cs} - \eta_f A_f}\left[A_s - \frac{\dot{Q}_8}{U\left(T_6 - \frac{\dot{Q}_6}{UA_{6,7}} - \frac{\dot{Q}_8}{UA_{8,7}} - T_{ee}\right)}\right] \tag{7}$$

which is valid for every fin geometry.

The objective function of the optimization problem is the total fins volume, V, (i.e. the total fins mass), so as to guarantee the motor operating temperature (T_6) not to surpass a specified value. For pin fins:

$$V = 0.25N\pi d^2 L \tag{8}$$

where d and L are the pin diameter and pin length, respectively. An inequality constraint regarding the maximum shell surface area available for fins installation must be respected:

$$\frac{0.25N\pi d^2}{A_s} - 1 + s \leq 0 \tag{9}$$

where s is the ratio between the minimum free surface area and the total shell surface area, which was set to 0.2 and indicates that at least 20% of A_s must remain free. After the substitution of equation (7) into equation (8), the optimization problem is formulated as:

$$\min_{d,L} \frac{0.25\pi d^2 L}{A_{cs} - \eta_f A_f}\left[A_s - \frac{\dot{Q}_8}{U\left(T_6 - \frac{\dot{Q}_6}{UA_{6,7}} - \frac{\dot{Q}_8}{UA_{8,7}} - T_{ee}\right)}\right] \tag{10}$$

subjected to the inequality constraint represented by equation (9). In equation (10), η_f is given by equation (5), $A_{cs} = 0.25\pi d^2$, $A_f = \pi d L_c$ and $L_c = L + 0.25d$ [20]. The heat transfer rates rejected by the shell ($\dot{Q}_s$) and by the electric motor ($\dot{Q}_m$) are computed through the thermal model. The motor temperature (T_6) is set to a fixed value that corresponds to the upper threshold. In this paper, such a limit was considered to be 95°C.

The optimization algorithm is based on the penalty function method, in which the inequality constrained problem is converted into a sequence of approximate equality constrained problems. A composite function to be minimized is formed from the combination of the original objective function and a penalty function:

$$\min_{d,L,\varepsilon} \frac{0.25\pi d^2 L}{A_{cs} - \eta_f A_f}\left[A_s - \frac{\dot{Q}_8}{U\left(T_6 - \frac{\dot{Q}_6}{UA_{6,7}} - \frac{\dot{Q}_8}{UA_{8,7}} - T_{ee}\right)}\right] - \mu \ln \varepsilon \tag{11}$$

subjected to:

$$\frac{0.25N\pi d^2}{A_s} - 1 + s + \varepsilon = 0 \tag{12}$$

where the term $\mu \ln \varepsilon$ represents the logarithmic barrier function and ε and μ are the slack variable associated with the inequality constraint and the penalty parameter, respectively, both kept positive along the minimization process. As μ decreases to zero, the minima of original objective function and composite function coincide. The design variables of the approximate problem ($x = d$, L or ε) are updated in the iterative procedure as follows:

$$x^{k+1} = x^k + \Delta x \tag{13}$$

being subscript k the iteration number and Δx the step size, which is given by the multiplication of the step length and step direction. The lagrangian function is written for the approximate problem and the

first-order optimality conditions are applied, giving rise to a system of equations that is solved to compute the step direction. The step length is calculated to decrease a merit function as described in [19]. Additional details of the optimization algorithm are available in the MATLAB Optimization Toolbox [19-21].

2.3. Solution procedure

Before the simulation starts, the thermal conductances $UA_{i,j}$ are adjusted using experimental data [7] of a baseline compressor. The global heat transfer coefficient between the compressor shell and the external environment U ($=UA_{8,ee}/A_s$) is determined. The motor efficiency is set to a lower value than that adopted in the baseline compressor and the thermal model is run for the first time. Naturally, the temperatures of the compressor components (especially the electric motor temperature) are increased when a lower-efficient motor is employed to drive the hermetic compressor. The heat transfer rates rejected by the shell and the electric motor are computed and used as input data for the optimization model, as shown in equation (10). The optimization is carried out and optimal values for fin geometric parameters are obtained (d^*, L^* and N^*). These are supplied to the thermal model, which is modified to encompass the effect of the fins. The thermal simulation is run again and new values of $\dot{Q}_s$ and T_m are calculated. Convergence is checked by comparing the updated motor temperature with the upper temperature threshold (which is 95°C in this case). If the deviation between these values is lower than 0.01°C, the simulation is finished. Otherwise, the updated $\dot{Q}_s$ is supplied to the optimization model and simulation continues until convergence is achieved. Figure 2 presents a flowchart of the simulation procedure.

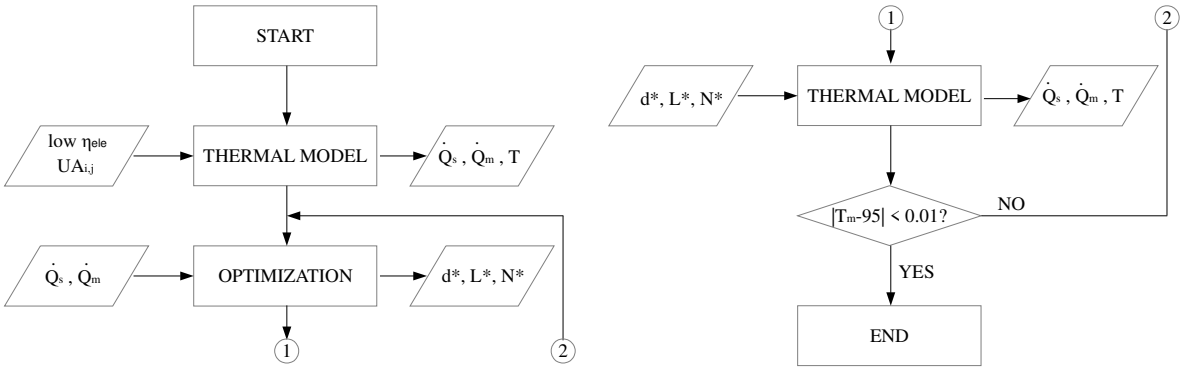

Figure 2. Simulation flowchart.

3. Results and discussion

3.1. Thermal model validation

Before presenting the results associated with the fin optimization, the thermal model is validated with measurements available in the literature [7]. The thermal conductances (UA) are adjusted for the operating condition defined by evaporating and condensing temperatures, T_e = -23.3°C and T_c = 54.4°C, respectively, and suction line (sl) and external environment (ee) temperatures equal to 32°C. Such values are presented in Table 2 and maintained fixed for simulations in other operating conditions. The hermetic compressor adopted in this study is employed for household and light commercial refrigeration applications. The volumetric displacement is 5.5cm³ and the nominal frequency is 50Hz. The refrigerant fluid is R290.

Table 2. Thermal conductances UA (W/K) adjusted at -23.3°C/54.4°C.

$\boldsymbol{UA_{1,7}}$	0.9021	$\boldsymbol{UA_{6,7}}$	4.396
$\boldsymbol{UA_{3,7}}$	0.6072	$\boldsymbol{UA_{8,7}}$	14.81
$\boldsymbol{UA_{4,7}}$	0.375	$\boldsymbol{UA_{8,ee}}$	2.115
$\boldsymbol{UA_{5,7}}$	1.116		

Figure 3 depicts experimental data and thermal model results for the electric motor temperature under nine operating conditions obtained from a combination of three evaporating temperatures (-35.0°C; -23.3°C; -10.0°C) and three condensing temperatures (45.0°C; 54.4°C; 70.0°C). The uncertainty associated with temperature measurements is approximately ±2°C with a 95% confidence interval [7]. Slight deviations are observed between simulation results and measurements for T_e = -23.3°C. On the other hand, the motor temperature is over- and under predicted when T_e = -10.0°C and T_e = -35.0°C, respectively. Such deviations can be explained by the adoption of fixed thermal conductances rather than considering the dependence on the compressor mass flow rate, which is very sensitive to the evaporating temperature. Despite this shortcoming, the maximum difference between measurements and predictions is lower than 4.5°C, which is satisfactory.

Still regarding Figure 3, the highest motor temperature is measured when the compressor operates at T_e = -23.3°C/T_c = 70.0°C and is approximately 95°C. Due to that, the fin optimizations are carried out under this operating condition, in which the baseline electric motor efficiency is found to be 78.5% [7]. If such a motor is replaced by a 70% efficient electric motor, the thermal model predicts a motor temperature equal to 106.8°C. The set of fins with minimum volume is then designed to be attached to the compressor shell and to ensure the motor temperature is maintained at 95°C even when operating with a low-efficiency motor. Two fin geometries are investigated herein: pins and rectangular-fins.

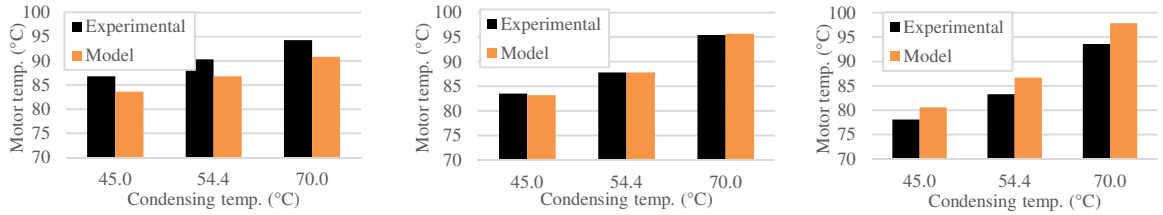

(a) T_e = -35.0°C (b) T_e = -23.3°C (c) T_e = -10.0°C

Figure 3. Measurements and simulation results for motor temperature.

3.2. Optimization results – pin fins configuration

Further the inequality constraint given by equation (9), lower bounds for pin length and pin diameter are set to zero ($L \geq 0$; $d \geq 0$), so as to avoid negative values for these parameters. The simulation is run and the optimal solution is given by L^* = 0.2mm, d^* = 1.5e-9mm and N^* = 1.01e16, which means that the fin diameter tends to zero whereas the number of fins tends to infinite.

In view of this infeasible configuration and since extremely thin fins can make the compressor handling more difficult, the lower bound for the fin diameter was gradually incremented and a parametric analysis was performed (Figure 4a). For all simulations, the optimal diameter coincided with the lower bound imposed and the shell free surface ratio (=1-NA_{cs}/A_s) was found to be equal to 0.2, which means that the inequality constraint given by equation (9) was active. As the optimal pin diameter is increased, the optimal pin length increases and the optimal number of pins decreases. The higher the optimal pin diameter, the higher the total volume and the mass of pins (for d^* = 2mm and d^* = 15mm, the total masses of pins are 0.19kg and 1.4kg, respectively). Such an outcome indicates that configurations with small pin diameters are likely to be adopted. However, the manufacture of a large amount of short pins may be unpractical. Hence, an additional analysis is carried out to evaluate the influence of the pin length on the optimal design.

Figure 4b shows optimal pin configurations as a function of the pin optimal length. In these simulations, the lower bound for the pin diameter was fixed in 2mm ($d \geq$ 2mm) and the lower bound for the pin length was gradually incremented. Except for the case in which the length lower bound is set to zero ($L \geq 0$), the optimal length coincided with the length lower bound. As the optimal pin length is increased, the optimal number of pins decreases and, since the optimal diameter remains the same (= 2mm), the shell free surface ratio increases. Due to the balance between pin length and number of pins, the optimum volume (or mass) of pins is roughly independent on the optimum pin length. Hence, possible pin configurations would be (i) d^* = 2mm; L^* = 3mm; N^* = 3900 (total pins mass = 0.19kg) or

(ii) $d^* = 2$mm; $L^* = 20$mm; $N^* = 430$ (total pins mass = 0.21kg). The choice is likely dependent on other design constraints such as the available space in the refrigerator to properly host the compressor and the difficulty of manufacturing a compressor shell with many pins.

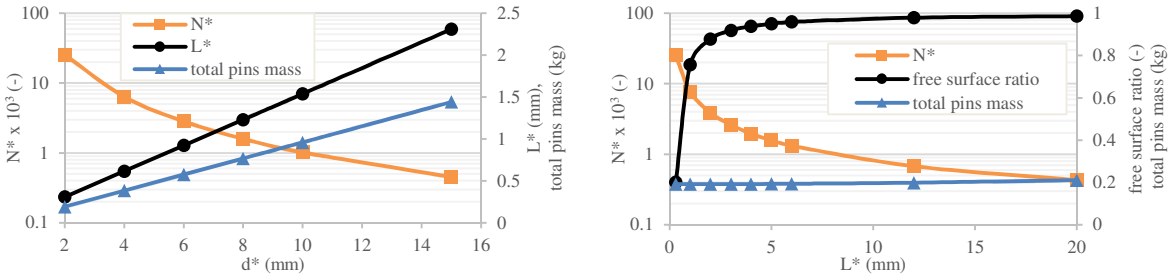

(a) (b)

Figure 4. Pin parameters as a function of the (a) pin optimal diameter and (b) pin optimal length.

A parametric analysis is carried out to assess the influence of the electric motor efficiency (η_{ele}) on the optimal pin configuration (Figure 5). Pin length and pin diameter lower bounds were fixed in 0 and 2mm, respectively ($L \geq 0$; $d \geq 2$mm). Also for these simulations, the optimal diameter coincided with the lower bound ($d^* = 2$mm). According to Figure 5a, the optimal number of pins and pin length increase with the motor efficiency decrement. This is an expected result, since the lower the efficiency, the larger the heat generation rate in the electric motor, requiring a greater amount of pins or longer pins to provide the motor cooling. For $\eta_{ele} < 0.7$, the free surface ratio is 0.2 (Figure 5b), which indicates that the inequality constraint is active and brings about the saturation of N^* (Figure 5a). When such a saturation takes place and η_{ele} still decreases, the rate of increase of L^* rises (as well as the total pins mass) so as to duly remove the heat generated and to meet the motor temperature requirement.

Still according to Figure 5a, the optimal solutions are formed by a large amount of short pins. Such pin configurations can be conveniently handled by incrementing the lower bound for the pin length. Thus, an optimum configuration can be obtained to meet manufacture constraints and with only a slight increase on the total pins mass (similarly to Figure 4b).

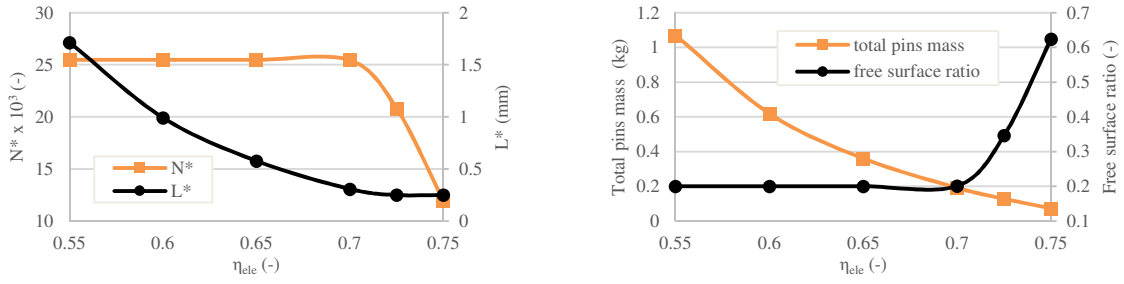

(a) (b)

Figure 5. Pin-fin configuration as a function of the motor efficiency. (a) Optimal pin length and number of pins and (b) total pins mass and free surface ratio.

3.3. Optimization results – rectangular-fins configuration

Four parameters are defined to fully characterize a rectangular-fin heat sink: width (w), thickness (t), length (L) and number of fins (N). Equations (9) and (10) should be modified to take into account the rectangular geometry. The fin width is made constant and equal to 80mm, since a wider fin could not be installed due to space limitation. On the other hand, a narrower fin could be set, but it does not affect the total volume of fins, as will be discussed below.

First, the lower bounds for fin length and fin thickness are both set to zero ($L \geq 0$; $t \geq 0$). As with the pin diameter, the optimum solution indicates that the fin thickness (t) tends to zero. Following the same procedure adopted for the pin-fins, the thickness lower bound was gradually incremented and a parametric analysis was performed, as shown in Figure 6a. The results are very similar to those obtained

with pin-fin configuration. As the optimal fin thickness increases, the optimal length increases and the optimal number of fins decreases. The total fin volume (or mass) is sensitive to the optimal fin thickness.

For a 1mm thick fin, the optimal length and optimal number of fins are 0.4mm and 739, respectively. Again, such a large amount of short fins may be undesired, so a parametric analysis is performed to evaluate the effect of the fin length (Figure 6b). In these simulations, the lower bound for the fin thickness was set to 0.5mm ($t \geq 0.5$mm) and the lower bound for the fin length was gradually incremented. The results follow the same trends observed in the pin-fins analysis, but some differences should be highlighted: (i) In the rectangular-fin configuration, the optimum number of fins (N^*) is found to be considerably lower than that predicted for pin-fins. This is due to the adoption of wide fins (w = 80mm). A narrower fin could be set without affecting the minimum total fins mass, since the optimum number of fins (N^*) would be increased proportionally. (ii) For a 2mm diameter, the total pins mass is nearly 0.2kg, whereas for a 0.5mm thick, the total rectangular-fins mass is close to 0.1kg. Such an outcome indicates that the optimal solution is conditioned to the smallest possible fin diameter or thickness, which depend on manufacture constraints.

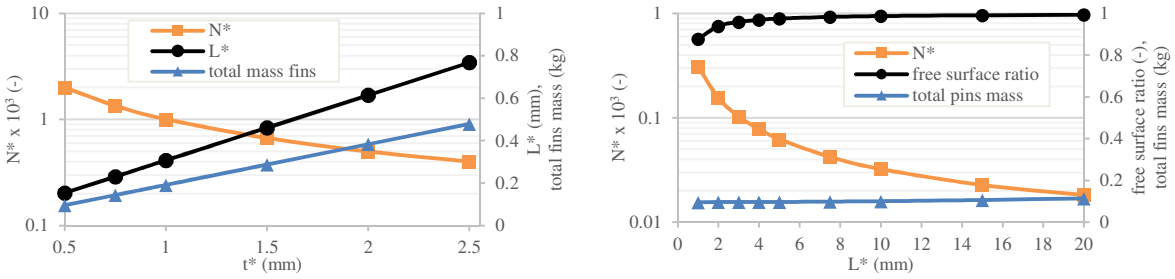

Figure 6. Rectangular-fin parameters as a function of the (a) optimal thickness and (b) optimal length.

4. Conclusions

This paper presented a simplified simulation model for optimization of fins on the shell of a hermetic reciprocating compressor driven by a low-efficient electric motor. The simulation is able to estimate a set of fins with minimum volume (or mass) that ensures motor operating temperature below an upper threshold. Pin and rectangular-fin geometries were investigated to demonstrate the applicability of the simulation model. It was observed that, as the motor efficiency is decreased, the optimal number of fins and optimal fin length increase whereas the optimum fin diameter tends to the lower bound value. Moreover, the relation between optimal fin length and optimal number of fins were seen to slightly affect the minimum volume (or mass) of fins. The optimal solutions were found to be conditioned to the smallest possible pin diameter and rectangular-fin thickness which are dependent on manufacture constraints. The simulation model proposed in this paper can be adopted in the thermal design of hermetic compressors.

References

[1] Meyer W A and Thompson H D 1990 An analytical model of heat transfer to the suction gas in a low-side hermetic refrigeration compressor. *Proc. Int. Compress. Eng. Conf. at Purdue*. West Lafayette, USA, pp. 898–907.

[2] Todescat M L, Fagotti F, Prata A T and Ferreira R T 1992 Thermal energy analysis in reciprocating hermetic compressors. *Proc. Int. Compress. Eng. Conf. at Purdue.* West Lafayette, USA, 1419-28.

[3] Cavallini A, Doretti L, Longo G A, Rosseto L, Bella B and Zannerio A 1996 Thermal analysis of a hermetic reciprocating compressor. *Proc. Int. Compress. Eng. Conf. at Purdue*. West Lafayette, USA, 535- 540.

[4] Rigola J, Pérez-Segarra C D and Oliva A 2000 Advanced numerical simulation model of hermetic reciprocating compressors. Parametric study and detailed experimental validation *Proc. Int. Compress. Eng. Conf. at Purdue* West Lafayette, USA, 23-30.

[5] Ooi K T 2003 Heat transfer study of a hermetic refrigeration compressor. *Appl. Therm. Eng.* **23** 1931-45.
[6] He Z, Xing Z, Chen W and Wang X 2013 Thermal and hydraulic analysis on the flow around the motor in semi-hermetic twin screw refrigeration compressors. *Appl. Therm. Eng.* **58** 114-124.
[7] Dutra T and Deschamps C J 2015a A simulation approach for hermetic reciprocating compressors including electrical motor modeling. *Int. J. Refrig.* **59** 168-181.
[8] Dutra T and Deschamps C J 2015b A thermal network model for induction motors of hermetic reciprocating compressors. *IOP Conf. Ser.: Mater. Sci. Eng.* **90** 012020.
[9] Kara S and Oguz E 2010 Thermal analysis of a small hermetic reciprocating compressor. *Proc. Int. Compress. Eng. Conf. at Purdue* West Lafayette, USA, 1307.
[10] Birari Y V, Gosavi S S and Jorwekar P P 2006 Use of CFD in design and development of R404a reciprocating compressor. *Proc. Int. Compress. Eng. Conf. at Purdue*. West Lafayette, USA, C072.
[11] Oliveira M J, Diniz M C and Deschamps C J 2017 Predicting the temperature distribution and the suction gas superheating of an oil-free linear compressor. *Journal of Process Mechanical Engineering.* **231** (1) 47-56.
[12] Posch S, Hopfgartner J, Dür L, Eichinger M, Stangl S and Almbauer R 2018 Thermal loss analysis of hermetic compressors using numerical simulation. *Appl. Therm. Eng.* **130** 1580-89.
[13] Schreiner J E, Ribas Jr, F A, Deschamps, C J, Barbosa Jr, J R, da Rosa, V H P 2009 Thermal management of a commercial reciprocating compressor through numerical simulation. *Proc. 7th Int. Conference on Compressors and Coolants*, Papiernicka, Slovak Republic.
[14] Chikurde R C, Loganathan E, Dandekar D P and Manivasagam S 2002 Thermal Mapping of Hermetically Sealed Compressors Using Computational Fluid Dynamics Technique. *Proc. Int. Compress. Eng. Conf. at Purdue*. West Lafayette, USA, C6-4.
[15] Raja B, Sekhar S J, Lal D M and Kalanidhi A 2003 A numerical model for thermal mapping in a hermetically sealed reciprocating refrigerant compressor. *Int. J. Refrig*. **26** (6) 652-658.
[16] Wu J, Hu J, Chen A, Mei P, Zhou X and Chen Z 2016 Numerical analysis of temperature distribution of motor-refrigerant in a R32 rotary compressor. *Appl. Therm. Eng.* **95** 365-373.
[17] Schreiner J E 2008 *Development of methodologies for the analysis of thermal management solutions for reciprocating compressors.* MSc Dissertation Thesis, Federal University of Santa Catarina, Brazil.
[18] Bergman T L, Lavine A S, Incropera F P and DeWitt D P 2011 *Fundamentals of heat and mass transfer.* John Wiley & Sons 7th ed.
[19] Waltz R A, Morales J L, Nocedal J and Orban D 2006 An interior algorithm for nonlinear optimization that combines line search and trust region steps. *Math. Program.* **107** 3 391-408.
[20] Byrd R H, Gilbert J C and Nocedal J 2000 A trust region method based on interior point techniques for nonlinear programming. *Math. Program.* **89** 149-185.
[21] Byrd R H, Hribar M E and Nocedal J 1999 An interior point algorithm for large-scale nonlinear programming *SIAM J. Optim.* **9** (4) 877-900.